Accepted manuscript. Published in IEEE Journal of Photovoltaics (2015), 10.1109/jphotov.2015.2407152

Passivation induced cavity defects in laser doped selective emitter Si solar cells – Formation model and recombination analysis

Christian Geisler, Sven Kluska, Sybille Hopman, Johannes Giesecke, and Markus Glatthaar

***Abstract*—Laser induced selective Si doping and simultaneous ablation of a dielectric passivation layer is a promising technology to create efficient and cost effective solar cells. In this paper, the electrical quality of emitters produced with a 532 nm continuous wave laser will be discussed using elaborate analysis of QSSPC measurements. It will be shown that these emitters cause good charge carrier shielding which leads to emitter saturation current densities as low as 240 fA/cm^2 for unpassivated surfaces. If a SiN_x layer is present during laser-doping the emitter recombination increases by a factor of three. This detrimental effect is put down to the formation of micro cavities within the recrystallized Si. A model of the ablation mechanism and cavity formation for long laser pulses is proposed, with the experimental data in this work serving as a limiting case for long irradiation lengths.**

***Index Terms*—solar cells, laser doping, emitter recombination, laser induced defects, SiNx ablation.**

I. Introduction

LASER processing is an important tool for selective Si doping and dielectric ablation. It is seen as an enabling technology for high performance and cost effective solar cells. During cell production laser doping is usually performed after the deposition of an dielectric anti-reflection-coating (typically SiN_x) [1]–[3] but can alternatively be performed before dielectric deposition which results in a higher quality of the laser doped Si [4]. The advantage of laser processing after dielectric deposition is simultaneous and self-aligned selective dielectric ablation and laser doping. If the laser doping is performed before dielectric deposition an additional process step for the patterning of the dielectric is needed. In order to calculate which processing sequence yields higher efficiencies or better cost-effectiveness, the impact of the presence of a dielectric coating during laser doping on emitter recombination needs to be understood and precisely measured.

Recent studies indicate that the removal of a thin SiN_x film by means of ultra short laser pulses occurs via a lift-off mechanism [5]. Here the laser irradiation is absorbed near the surface of the Si substrate, the Si below the film melts and evaporates rapidly, resulting in a lift off of the thin film atop. In the case of longer laser pulses the ablation mechanism relies on melting the underlying Si substrate and heating the SiN_x layer atop via thermal conduction above its decomposition temperature [6], [7]. Both ablation mechanisms rely on melting the underlying Si which is followed by rapid re-crystallization. Due to re-crystallization velocities in the order of m/s proper choice of processing parameters can only minimize the laser induced crystal damage but cannot prevent it entirely [1], [4], [5], [8], [9]. Laser processes with long pulses are also suitable for laser induced selective doping [10]–[12]. Here dopants from an external source diffuse rapidly within the liquid phase of the molten Si. Especially, green ns-pulsed or continuous wave (cw) lasers prove to be suited for selective doping in solar cell applications. In recent years many groups have combined the selective laser doping and selective laser ablation into a single process step [3], [10], [13]. Doing so, Hameiri et al. [4] have observed that emitter quality is reduced if SiN_x ablation and doping are combined into a single step. It is assumed that this is caused by a thermal expansion mismatch between SiN_x and Si. Especially, cw-laser processing of a Si wafer after SiN_x deposition is a promising tool to create a selective emitter and simultaneously ablate the dielectric. Due to the Si melt duration in the order of microseconds and particular melt circulation [14] deep and homogeneous pn-junctions are formed.

In this work the SiN_x ablation mechanism of cw-laser processing and the impact of the simultaneous doping on carrier lifetimes will be investigated. It will be shown that great care needs to be taken if recombination properties are to be measured using asymmetric samples and lifetime-testers based on xenon flash illumination, which are common in laboratory and production environments. It will be demonstrated that the presence of a SiN_x layer promotes the formation of cavities within the re-solidified Si and significantly increases the emitter saturation current density. As a last point a model will be presented that explains the observed cavity formation and lifetime reduction in cw-laser processing. The proposed mechanism explains the dielectric ablation and considers defect formation beyond induced stress by thermal expansion mismatch.

II. Experimental

The quality of a laser doped Si is examined by measuring the emitter saturation current density of laser-doped (LD) emitters. A distinction was made between doping of bare Si wafers and Si wafers with a SiN_x anti-reflection coating.

A. Sample preparation

A 120 Ω emitter was created on both sides of alkaline textured 240 μm thick 1 Ωcm p-type fz-Si wafers using a

C. Geisler, S. Kluska, S. Hopman, J. Giesecke and M. Glatthaar are with the Division Solar Cells - Development and Characterization, Fraunhofer Institute of Solar Energy Systems, Freiburg, Germany e-mail: christian.geisler@ise.fraunhofer.de .

Manuscript received xxxx; revised xxxx

$POCl_3$ furnace diffusion process. Subsequently, a 75 nm thick SiNx film was deposited by plasma-enhanced chemical-vapor deposition (PECVD). The batch of wafers was split into two groups "LD-SiNx" and "LD-bare". The front side of the "LD-SiNx" wafers were spin-coated with 30% H_3PO_4 for 60 s at 3000 RPM resulting in a 1.5 μm thick liquid phosphorous dopant layer. A 532 nm continuous wave laser (Spectra Physics Millennia Prime) guided by a galvometer scanning head (Scanlabs Intelliscan 20) was used to locally dope and pattern the sample. The laser beam was focused through an f-theta lens to a 15 μm ($1/e^2$ diameter) spot onto the front surface of the wafer. The 15 W laser spot was scanned across the sample at velocity of 5 m/s. The laser power is sufficient to simultaneously ablate the SiN_x and create 12 μm wide and 3 μm deep highly doped lines with a sheet resistance of 15 Ω. Each wafer was subdivided into four quadrants (4 cm×4 cm) with varying coverage of laser treated area: unprocessed reference, 4 % coverage (resembling the average coverage of a solar cell with a selective emitter structure), 20 % coverage and full coverage using a line to line hatch distance of 5 μm. With the exception of the unprocessed reference quadrant the single sided laser processing created asymmetrical samples, regarding front and rear side of the sample. In order to remove the dopant film residue the wafers were cleaned in a DI-water rinser. Subsequently, the SiN_x film was removed using 20 % HF from all wafers of both groups. The "LD-bare" group was laser doped after SiN_x removal in the same fashion as described above. After that the samples were coated on both sides with a silicon rich oxinitride (SiriON) [15] layer by PECVD and fired at 650° C to enhance the hydrogen passivation.

B. Emitter saturation current densities

The injection dependent effective charge carrier lifetime τ_{eff} was measured at low level injection by means of the quasi-steady-state photoconductance (QSSPC) method [16]. The optical properties of the planar laser treated and the textured furnace diffused surfaces have been corrected for by using OPAL [17]. With (without) the SiriON dielectric the light coupling into the planar sample is a factor of 0.94 (0.68) lower than the reference solar cell and the coupling of the textured sample is a factor of 1.06 (0.93) higher (lower). From τ_{eff} at $\Delta n_{av} = 3 \cdot 10^{15}\,\text{cm}^{-3}$ the j_{0e} of the laser-doped emitter is calculated as described in detail below. Subsequently the SiriON layer was removed using 20 % HF and the j_{0e} measurement of the unpassivated emitter was repeated. After this the laser-doped emitter dopant profile has been measured using the electrochemical capacitance-voltage (ECV) technique.

C. Delineation etch and microscopy studies

Cross sections of laser processed lines from the "LD-SiNx" and the "LD-bare" group have been examined using a scanning electron microscope (SEM). Additionally, the samples have been etched in secco etchant [18] for 15 s to delineate crystal defects and examined using SEM.

III. Theory and methodology of j_{0e} determination

In order to extract the emitter saturation current density j_{0e} from QSSPC measurements the following simplified relation is commonly used [19]:

$$\frac{1}{\tau_{\text{eff}}} = \frac{1}{\tau_B} + \frac{N_a\,(j_{0e,0} + j_{0e,W})}{qWn_i^2} \tag{1}$$

with j_{0e} of the front $j_{0e,0}$ and rear side $j_{0e,W}$, the effective charge carrier lifetime τ_{eff}, bulk recombination lifetime τ_B, base doping concentration N_a, elementary charge q, wafer thickness W and intrinsic carrier concentration n_i. This expression is accurate if the excess charge carrier density is independent of the position within the wafer: $\Delta n(z) \approx \text{const.}$ [20].

For the experimental data analyzed in this work the error introduced by this approximation exceeded 30 % during the analysis of the "LD-SiNx" group, which would have lead to significant underestimation of the saturation current densities of the laser doped emitters. In the following the steady-state continuity equation which describes the distribution of excess charge carriers $\Delta n(z)$ is solved to accurately extract the j_{0e} of the laser doped structures.

In the case of steady-state photoexcitation $\Delta n(z)$ is governed by the time-independent continuity equation:

$$-D\frac{d^2\Delta n(z)}{dz^2} + \frac{\Delta n(z)}{\tau_B} = g(z) \tag{2}$$

where D is the ambipolar diffusion coefficient, and $g(z)$ is the photogeneration along the depth z of a laterally homogeneous sample. Illumination of the front side of the wafer using monochromatic light with photo current j_λ and absorption coefficient in Si α_λ results in the excess carrier generation rate:

$$g_\lambda(z) = j_\lambda \alpha_\lambda \exp(\alpha_\lambda z). \tag{3}$$

A general solution of Eq. 2 for monochromatic excitation can be determined by evaluating the boundary conditions at the front ($z = 0$) and rear ($z = W$) surface of the sample, representing the loss of excess minority carriers at the surfaces:

$$\begin{aligned} D\frac{d\Delta n(z)}{dz}\Big|_{z=0} &= S_0 \Delta n(z=0) \\ D\frac{d\Delta n(z)}{dz}\Big|_{z=W} &= -S_W \Delta n(z=W) \end{aligned} \tag{4}$$

S_0 and S_W are the effective surface recombination velocities of the front and rear surfaces. They are the key values to extract from the QSSPC measurement in order to determine the emitter quality in terms of an emitter recombination current density. The solution of Eq. 2 Δn_λ for a given $g_\lambda(z)$ can be found in the appendix.

The excess carrier density Δn_λ can now be calculated for monochromatic excitation for a given D, τ_B, α_λ, j_λ, W, S_0 and S_W. In order to determine $\Delta n(z)$ during illumination with a broad spectrum of wavelengths, as it is the case during QSSPC measurements, the monochromatic solutions can be superposed:

$$\Delta n(z) = \sum_\lambda \Delta n_\lambda(z) \tag{5}$$

Accordingly, the total generation becomes:

$$g(z) = \sum_{\lambda} g_{\lambda}(z) \tag{6}$$

The primary value measured by the QSSPC technique is the effective charge carrier lifetime τ_{eff} which is defined as the ratio between excess carrier density and generation rate:

$$\tau_{\text{eff}}(\Delta n_{\text{av}}) := \frac{W \Delta n_{\text{av}}}{\int_0^W dz g(z)} \tag{7}$$

at an averaged excess minority carrier concentration:

$$\Delta n_{\text{av}} = (1/W) \int_0^W dz\, \Delta n(z) \tag{8}$$

With a known Δn_{av} ($= 3 \cdot 10^{15}\,\text{cm}^{-3}$), ambipolar diffusion coefficient D ($= 21.9\,\text{cm}^2\text{s}^{-1}$), and a bulk lifetime τ_B ($= 10^{-3}\,\text{s}$), the effective lifetime τ_{eff} can now be calculated as a function of S_0 and S_W using spectral irradiance data for the xenon flash used [21].

In the case of the symmetrical furnace diffused sample both surfaces have the same recombination velocity $S_0 = S_W$ which allows the determination of S_W ($= 30\,\text{cm/s}$ for the SiriON passivated sample) from the measured effective lifetime τ_{eff} ($= 290\,\mu s$).

For diffused wafers the surface recombination velocity at an imaginary surface at the base side of the space charge region is equivalent to the recombination current in the emitter [22]:

$$S = j_{0e} \frac{N_a + \Delta n}{q n_i^2} \tag{9}$$

with base doping concentration N_a, elementary charge q, and intrinsic carrier concentration n_i ($= 8.3 \cdot 10^9\,\text{cm}^{-3}$ at 25° C). Accordingly, S_W of the SiriON passivated furnace diffused emitter corresponds to an emitter saturation current of $j_{0e,W} = 18\,\text{fA/cm}^2$ which is in good agreement with earlier experiments [23]. This value is now used to determine the surface recombination velocity S_0 and emitter saturation current density j_{0e} of the laser processed surfaces of the asymmetrical samples from the measured τ_{eff}.

IV. Results and Discussion

In the first section the j_{0e} values of the samples produced according to the scheme shown in Figure 1 are discussed. After that laser induced defects are studied using delineation etching and SEM analysis. This leads to a model for the SiN_x ablation which is presented in the last section.

A. Emitter saturation current densities

Figure 2 shows the j_{0e} of the laser treated surface as a function of the coverage with laser lines. The plot collects j_{0e} of the passivated as well as unpassivated samples from the "LD-bare" and "LD-SiNx" group. The j_{0e} of the passivated laser-doped emitters were determined by fitting a line through 0%, 4% and 20% coverage (green and blue triangles) and extrapolating to full coverage [8], [24]. This value determined from the fit is with $195 \pm 3\,\text{fA/cm}^2$ for the "LD-bare" group significantly smaller than the $233 \pm 5\,\text{fA/cm}^2$ measured at full

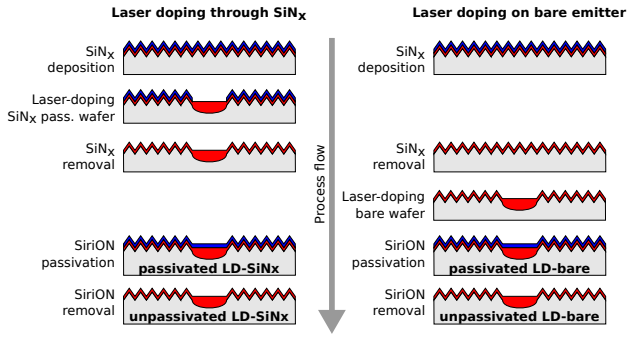

Fig. 1. Processing scheme for the samples produced for this experiment.

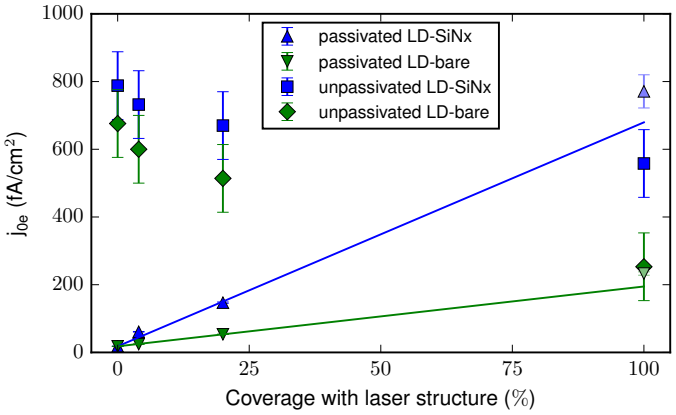

Fig. 2. Effective j_{0e} as a function of the coverage with laser-doped emitter of the "LD-bare" (green) and the "LD-SiNx" (blue) group (Schematic of process groups cf. Fig. 1). Triangles represent j_{0e} of SiriON passivated samples whereas squares represent the corresponding j_{0e} with unpassivated surfaces. In the case of the SiriON samples j_{0e} increases rapidly with laser-doped emitter coverage, whereas in the unpassivated case the laser-doped emitter has a lower j_{0e} than the high efficiency furnace diffused emitter.

coverage. Full coverage is achieved by a narrow hatch of $5\,\mu m$ that is smaller than the laser line width of $12\,\mu m$. As a result every point on the surface is molten and re-crystallized at least two times. This additional re-crystallization is expected to be the cause for an increased amount of imperfections and increased j_{0e} [25]. Also in the "LD-SiNx" group the j_{0e} from the fit is with $680 \pm 58\,\text{fA/cm}^2$ smaller than the measured $771 \pm 49\,\text{fA/cm}^2$ at full coverage, however this difference is not significant.

In either case the emitter recombination is strongly increased if a SiN_x dielectric is present during laser treatment, which will be discussed in detail in the following section. In the unpassivated case i.e. after the removal of the SiriON dielectric using HF, the measured lifetime decreased dramatically ($\approx 10\,\mu s$) mostly due to the increased recombination of the unpassivated furnace diffused emitter to $j_{0e,W}^{\text{unpass}} \approx 750\,\text{fA/cm}^2$. Due to enhanced carrier shielding j_{0e}^{unpass} decreases with the laser-doped emitter coverage. The benefit of deep pn-junctions with regard to shielding carriers from a recombinative surface becomes evident if j_{0e} calculated using EDNA [26] from the laser-doped emitter profile for a well passivated case (S_{surf}= 10cm/s) j_{0e} =120 fA/cm^2 is

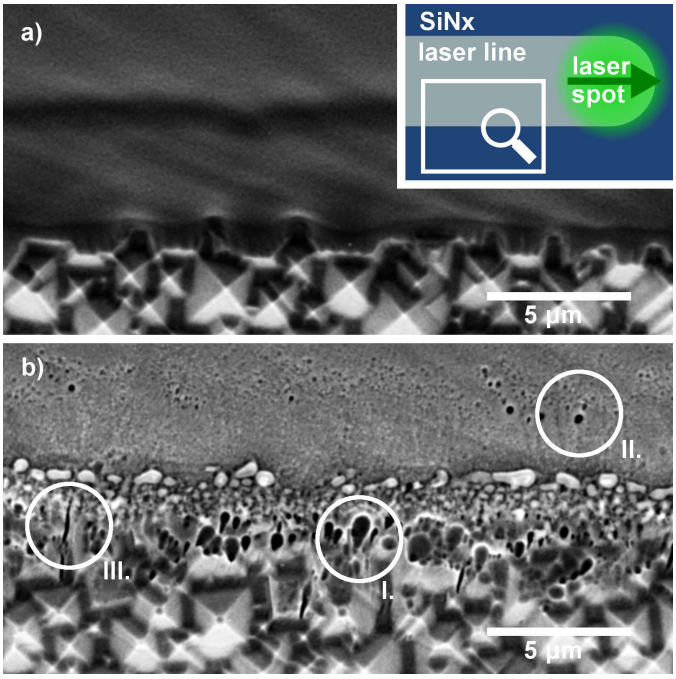

Fig. 3. Top view SEM images of the edge of a laser line from the "LD-bare" (a) and "LD-SiNx" (b) group after secco delineation etching. The inset shows a schematic of a laser line and indicates the area imaged in a) and b) as well as the moving direction of the laser spot. Only the "LD-SiNx" sample (b) shows a large number of etch pits which are categorized into three classes. I: large round or tear-shaped pits at the edge of the laser line; II: round etch pits in the center of the line; III: cracks at the edge and region of low irradiation.

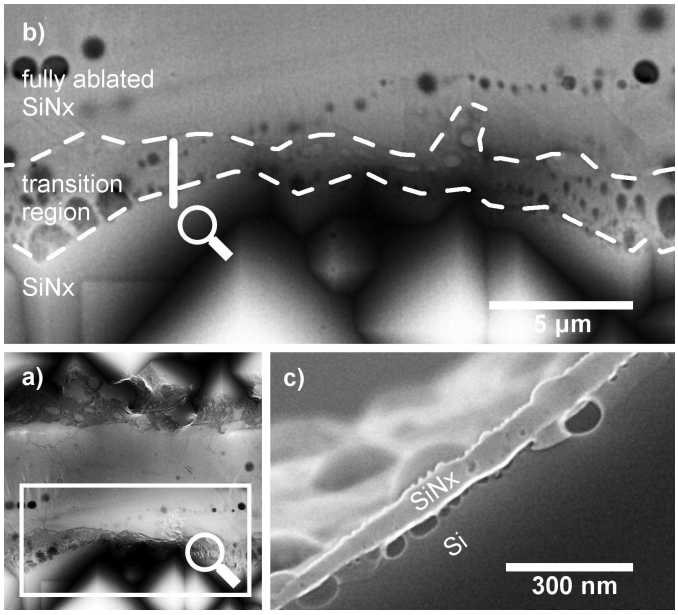

Fig. 4. Top view SEM image of a laser line from the "LD-SiNx" group using secondary electrons (a). In this imaging mode three regions can be identified by their respective surface morphology: un-irradiated SiN_x, partly ablated transition region, and fully ablated SiN_x. These region have been mapped from (a) to close-up (b) showing the corresponding features using back-scatter electrons. A sampling depth of 1.5 μm allows detection of cavities within the Si in the transition region and in the fully ablated region. At a position similar to the vertical bar in (b) a cross section was polished in the transition region (c). The cavities in this region are located remarkably close to the SiN_x layer.

compared to j_{0e} for the unpassivated case (S_{surf}=10^7 cm/s) j_{0e}^{unpass} =180 fA/cm^2. In comparison to the furnace diffused emitter the quality of the passivation layer has only a minor influence on the emitter recombination. It needs to be noted that the trend of decreasing j_{0e}^{unpass} with laser-doped emitter coverage is also present in τ_{eff} but due to high $j_{0e,W}^{unpass}$ the absolute values of j_{0e}^{unpass} calculated from τ_{eff} are of reduced precision as indicated by the large error bars in fig. 2.

B. Delineation etch and microscopy studies

Figure 3 shows SEM images of laser line edges of the "LD-bare" and "LD-SiNx" group after delineation etching. In the "LD-bare" case (a), where laser doping was performed on a bare surface, no etch pits are observed indicating a low crystal defect density. This is in agreement with the measured j_{0e} (195 fA/cm^2) which is on a similar level as the j_{0e} determined from the ECV profile (120 fA/cm^2) using EDNA. As the EDNA calculation includes only auger recombination the difference to the measured value is an indicator of crystal damage in the emitter. In the "LD-SiNx" case (b) the additional SiN_x layer present during laser treatment lead to a high etch pit density which is in agreement with the increased measured j_{0e} (680 fA/cm^2) and the high difference to the j_{0e} calculated (120 fA/cm^2) using EDNA. Most of the etched pits are round or tear-shaped and are located at the edge of the laser line, in the transition region between full SiN_x ablation and non-irradiated SiN_x (cf. fig. 3 (b) type I.).

This crystal damage on the edge of the laser line was observed before and is attributed to the thermal expansion mismatch between SiN_x and Si [1], [25], [27], [28]. The referenced works suggest that during heating, the SiN_x layer puts the underlying Si under tensile stress and induces crystal defects. Hameiri et al. [4] showed that a SiO_2/ SiN_x double layer reduces this detrimental effect. They argue that the thermal expansion mismatch between SiO_2 and Si puts the underlying Si under compression which induces fewer defects during cooling. The expansion mismatch may explain the observed etch pits and cracks in the transition region but fig. 3 also reveals defects in the center of the laser line (cf. fig. 3 (b) type III.), which cannot solely be caused by a thermal expansion mismatch.

To investigate the origin of the defects in the edge region SEM imaging was performed on a "LD-SiNx" sample directly after the laser treatment. Using an electron energy of 30 keV and a backscatter electron detector (BSD) resulted in a sampling depth of 1.5 μm which allowed to image material properties up to this depth. Figure 4 (a) shows an overview of the laser line using secondary electron imaging. In this imaging mode three regions of varying SiN_x ablation can be identified: un-irradiated SiN_x, partly ablated transition region, and fully ablated SiN_x. These regions have been mapped to the close-up (b). The image from the BSD reveals that the pits which were exposed by the delineating etch were already present as cavities within the Si in the edge region as well as the central area of the laser line. Cavities appear in the BSD image as regions with reduced signal due to increased material penetration depth and thus reduced backscattering probability. A SEM image of a cross-section in the transition region is

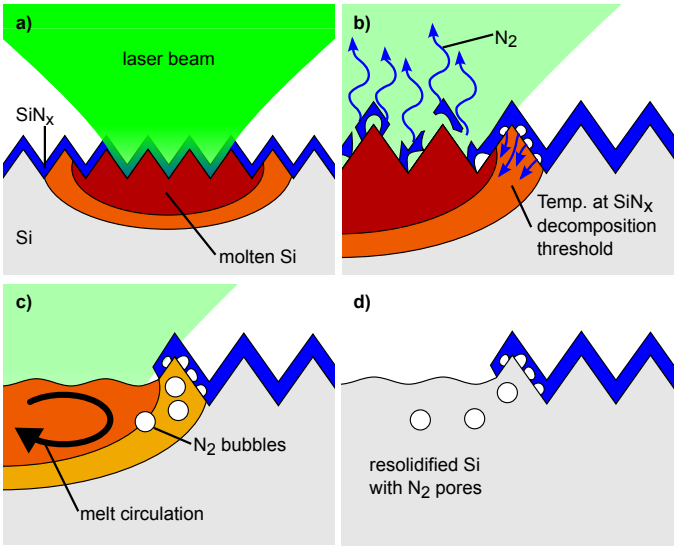

Fig. 5. Scheme of SiN_x ablation using laser processing. Laser melting of Si (a) leads to indirect heating and decomposition of SiN_x layer atop the molten pool (b). Due to reduced temperature of the pool in the transition region the SiN_x layer is only partly decomposed. N_2 from the decomposition of SiN_x is released as bubbles into the molten Si where they are transported by melt circulation (c). After re-solidification the bubbles are frozen in place (d).

shown in fig. 4 (c). On top of the Si the thin SiN_x passivation layer is visible. This layer is slightly bulged and deformed indicating that is has been exposed to temperatures close to its decomposition temperature. A string of cavities is located just below the SiN_x layer, which suggests the assumption that the cavities originate from decomposed SiN_x at the underside of the SiN_x passivation layer. This leads to a model of the ablation and defect formation which will be discussed in the following.

C. Model of SiN_x ablation and cavity formation

The observation of the strongly increased recombination as well as the formation of cavities in the laser-doped emitter lead to a model of the SiN_x ablation mechanism using laser processing as depicted in figure 5. The SiN_x dielectric is transparent at wavelengths down to the UV regime. At wavelengths laser processing is typically performed, only a minute fraction of irradiation is absorbed directly within the thin SiN_x layer. For green lasers at 532 nm this fraction is 0.3 % and for UV laser processing at 355 nm it is 2.8 %. The laser irradiation is mostly absorbed in the underlying Si. At sufficient laser power the Si is molten in a pool shape with the highest temperature in the center and decreasing to the sides. This is illustrated in fig. 5 (a). Conductive heat transfer results in an indirect heating of the SiN_x atop the molten pool. If the SiN_x exceeds a temperature of 2150 K it decomposes into liquid Si and gaseous N_2 [29], [30]. In the center region the energy input into the SiN_x layer is sufficient to fully decompose the SiN_x and the released N_2 can freely escape into the atmosphere. The temperature of the molten Si pool decreases laterally and at some distance from the center the heat conducted to the SiN_x is insufficient to fully decompose the SiN_x. In this transition region only a fraction of the SiN_x layer which is in direct contact with the molten Si may be decomposed as illustrated in (b). As the remaining solid SiN_x is still atop the decomposed part the gaseous N_2 is released as a bubble into the molten Si. The width of this transition region and thus the extent of bubble formation depends on the wavelength and shape of the laser spot as well as the effective irradiation duration. A lateral temperature gradient at the surface of the molten pool causes a gradient in surface tension. This surface tension gradient leads to a circular mass transfer of the molten Si within the molten pool [14] as illustrated in (c). This flow of molten Si transports the bubbles away from the transition region towards the center of the laser line. As the laser processed area cools down the bubbles are frozen within the re-solidified Si. This is illustrated in (d).

In this work cw-laser doping serves as an example with a Gaussian intensity profile and an effective irradiation dwell time of 3 μs. For this case Blecher et al. [14] have predicted strong melt circulation which are in agreement with high junction depths and the proposed bubble transport. The presence of cavities leads to additional unpassivated surface area within the emitter which is particularly detrimental if these recombination active surfaces are close to the space charge region.

Bubble formation depends on the temperature distribution on the surface of the molten pool and can be reduced, if the transition region with incomplete SiN_x ablation is narrowed. This can be achieved by shorter irradiation duration, which reduces heat transfer to the SiN_x layer in the transition region. Using a laser system with a flat-top intensity profile will also narrow the transition region. Melt circulation, which causes the transport of bubbles within the molten pool, increases with the temperature gradient at the surface of the molten pool and with the duration of irradiation. Like bubble formation melt circulation is reduced if short laser pulses and flat-top intensity profiles are used.

In earlier experiments using green laser pulses with a Gaussian intensity profile and a pulse duration of 80 ns no cavities in the center region of the laser line have been observed. Applying the proposed model for cavity formation, this can be explained by shorter melt duration and reduced melt circulation. However, at present it is not clear at exactly what process parameters the bubble formation becomes substantial and significantly reduces the emitter quality. The experiment shown in this work merely represents a case that clearly is affected by process induced cavities in the laser doped emitter.

V. Conclusion

The discussion of the recombination quality of laser-doped emitters presented in this work is based on the solution of the steady-state continuity equation for excess charge carriers. This method of extracting j_{0e} values exceeding $\approx 100\,\mathrm{fA/cm^2}$ from QSSPC lifetime measurements circumvents systematic errors introduced by commonly used approximations. It was found that j_{0e} of a laser-doped emitter with a SiN_x layer present during laser processing is more than three times as high as the j_{0e} of a laser-doped emitter which was created before the deposition of the SiN_x layer. Further, it was shown that laser-doped emitters are effectively shielding charge carriers

from unpassivated or metallized surfaces which results in lower recombination compared to a homogeneous emitter formed via furnace diffusion.

Using SEM imaging and delineation etching, defects have been located at the edge of the laser line. In earlier publications these defects have been attributed to a thermal expansion mismatch between Si and SiN_x. SEM imaging using backscatter electrons at high energies revealed that the majority of defects are already present after the laser process in the form of micro cavities. This cannot result from a mere expansion mismatch. SEM imaging on a cross section of a laser line suggests a model of SiN_x ablation for laser processing where the SiN_x layer is indirectly heated from the molten Si. At the edge of the laser line the SiN_x is only partly decomposed into gaseous N_2 which is released into the liquid Si as bubbles. Circulation currents driven by a temperature gradient at the surface transports these bubbles within the molten pool. The detrimental effect of the SiN_x layer can be put down to the fact that these micro cavities introduce additional unpassivated surfaces to the laser-doped emitter or additional recombination active defects within the emitter.

The precise influence of the laser process parameters on cavity formation, transport and emitter quality is not fully understood. Compared to laser processing using pulsed lasers, the pool depth as well as the irradiation length is rather large for the experimental parameters presented in this paper. However, the findings suggest that large melt pools and long irradiation lengths can create emitters with excellent charge shielding properties if cavity formation can be prevented, as can be seen for samples that were laser-doped before SiN_x deposition. The optimal trade-off between bubble formation and charge shielding may be achieved by increasing the scanning speed of a laser spot with a flat-top intensity profile or by creating the laser-doped emitter before SiN_x deposition as presented in [13].

APPENDIX
STEADY-STATE SOLUTION OF THE CONTINUITY EQUATION

A general solution of Eq. 2 for monochromatic excitation (Eq. 3) is [31]:

$$\Delta n_\lambda(z) = A_\lambda e^{z/L} + B_\lambda e^{-z/L} - \frac{j_\lambda \alpha_\lambda}{D(\alpha_\lambda^2 - L^{-2})} e^{-\alpha_\lambda z} \quad (10)$$

with the diffusion length of the minority carriers $L = \sqrt{D\tau_B}$. The coefficients A_λ and B_λ are determined by inserting Eq. 10 into the boundary conditions (Eq. 4). The resulting system of equations is:

$$\begin{pmatrix} S_0 - \frac{D}{L} & S_0 + \frac{D}{L} \\ (S_W + \frac{D}{L})e^{W/L} & (S_W - \frac{D}{L})e^{-W/L} \end{pmatrix} \begin{pmatrix} A_\lambda \\ B_\lambda \end{pmatrix} = \frac{\alpha_\lambda j_\lambda}{\alpha_\lambda^2 - L^{-2}} \begin{pmatrix} \frac{S_0}{D} + \alpha_\lambda \\ (\frac{S_W}{D} - \alpha_\lambda)e^{-\alpha_\lambda W} \end{pmatrix} \quad (11)$$

Expression in terms of matrix elements

$$\begin{pmatrix} a_{11} & a_{12} \\ a_{21} & a_{22} \end{pmatrix} \begin{pmatrix} A_\lambda \\ B_\lambda \end{pmatrix} = \begin{pmatrix} b_1 \\ b_2 \end{pmatrix} \quad (12)$$

yields the coefficients

$$A_\lambda = \frac{b_1 a_{22} - b_2 a_{12}}{a_{11} a_{22} - a_{21} a_{12}} \quad (13)$$

$$B_\lambda = \frac{b_1 a_{21} - b_2 a_{11}}{a_{21} a_{12} - a_{11} a_{22}}. \quad (14)$$

ACKNOWLEDGMENT

The authors would like to thank the PV-TEC and clean room team at Fraunhofer ISE for sample processing. This work was funded by the German Federal Ministry for the Environment, Nature Conservation and Nuclear Safety in the frame of the project rEvolution (FKZ 0325586B).

REFERENCES

[1] B. Hallam, S. Wenham, C. M. Chong, A. Sugianto, L. Mai, M. Edwards, D. Jordan, and P. Fath, "Record large area p-type CZ production cell efficiency of 19.3% based on LDSE technology," in *IEEE Journal of Photovoltaics*, vol. 1, no. 1, 2011, p. 43.

[2] Z. Hameiri, L. Mai, A. Sproul, and S. R. Wenham, "18.7% efficient laser-doped solar cell on p-type Czochralski silicon," *Applied Physics Letters*, vol. 97, no. 22, p. 222111, 2010.

[3] S. Kluska, C. Fleischmann, A. Büchler, W. Hördt, C. Geisler, S. Hopman, and M. Glatthaar, "Micro characterization of laser structured solar cells with plated NiAg contacts," *Solar Energy Materials and Solar Cells*, vol. 120, pp. 323–331, Jan. 2014.

[4] Z. Hameiri, T. Puzzer, L. Mai, A. B. Sproul, and S. R. Wenham, "Laser induced defects in laser doped solar cells," *Progress in Photovoltaics: Research and Applications*, vol. 19, no. 4, pp. 391–405, 2011.

[5] S. Hermann, T. Dezhdar, N.-P. Harder, R. Brendel, M. Seibt, and S. Stroj, "Impact of surface topography and laser pulse duration for laser ablation of solar cell front side passivating SiNx layers," *Journal of Applied Physics*, vol. 108, no. 11, p. 114514, 2010.

[6] G. Poulain, D. Blanc, A. Focsa, M. De Vita, K. Fraser, Y. Sayad, and M. Lemiti, "Characterization of laser-induced damage in silicon solar cells during selective ablation processes," *Materials Science and Engineering: B*, pp. 4–7, Dec. 2012.

[7] S. A. G. D. Correia, J. Lossen, M. Wald, K. Neckermann, and M. Bähr, "Selective Laser Ablation of Dielectric Layers," in *22nd European Photovoltaic Solar Energy Conference*, 2007, pp. 1061–1067.

[8] U. Jäger, S. Mack, C. Wufka, A. Wolf, D. Biro, and R. Preu, "Benefit of Selective Emitters for p-Type Silicon Solar Cells With Passivated Surfaces," *IEEE Journal of Photovoltaics*, vol. 3, no. 2, pp. 621–627, Apr. 2013.

[9] Z. Hameiri, L. Mai, T. Puzzer, and S. Wenham, "Influence of laser power on the properties of laser doped solar cells," *Solar Energy Materials and Solar Cells*, vol. 95, no. 4, pp. 1085–1094, Apr. 2011.

[10] B. Hallam, C. Chan, A. Sugianto, and S. Wenham, "Deep junction laser doping for contacting buried layers in silicon solar cells," *Solar Energy Materials and Solar Cells*, vol. 113, pp. 124–134, Jun. 2013.

[11] U. Jäger, D. Suwito, J. Benick, S. Janz, and R. Preu, "A laser based process for the formation of a local back surface field for n-type silicon solar cells," *Thin Solid Films*, vol. 519, no. 11, pp. 3827–3830, Mar. 2011.

[12] D. Kray, N. Bay, G. Cimiotti, S. Kleinschmidt, N. Kosterke, A. Losel, M. Sailer, A. Trager, H. Kuhnlein, H. Nussbaumer, C. Fleischmann, and F. Granek, "Industrial LCP selective emitter solar cells with plated contacts," in *35th IEEE Photovoltaic Specialists Conference*, 2010, pp. 667–671.

[13] C. Geisler, W. Hördt, S. Kluska, A. Mondon, S. Hopman, and M. Glatthaar, "Overcoming electrical and mechanical challenges of continuous wave laser processing for Ni–Cu plated solar cells," *Solar Energy Materials and Solar Cells*, 2014.

[14] J. J. Blecher, T. a. Palmer, T. DebRoy, and E. W. Reutzel, "Laser-silicon interaction for selective emitter formation in photovoltaics. I. Numerical model and validation," *Journal of Applied Physics*, vol. 112, no. 11, p. 114906, 2012.

[15] J. Seiffe, L. Gautero, M. Hofmann, J. Rentsch, R. Preu, S. Weber, and R. a. Eichel, "Surface passivation of crystalline silicon by plasma-enhanced chemical vapor deposition double layers of silicon-rich silicon oxynitride and silicon nitride," *Journal of Applied Physics*, vol. 109, no. 3, p. 034105, 2011.

[16] R. Sinton, A. Cuevas, and M. Stuckings, "Quasi-steady-state photoconductance, a new method for solar cell material and device characterization," in *25th European Photovoltaic Solar Energy Conference*, 1996, pp. 457–460.
[17] K. Mcintosh and S. Baker-finch, "OPAL 2 : Rapid Optical Simulation of Silicon Solar Cells," in *38th IEEE Photovoltaic Specialists Conference (PVSC)*, 2012.
[18] F. Secco d' Aragona, "Dislocation Etch for (100) Planes in Silicon," *Journal of The Electrochemical Society*, vol. 119, no. 7, p. 948, 1972.
[19] D. E. Kane and R. M. Swanson, "Measurement of the emitter saturation current by a contactless photoconductivity decay method," in *18th IEEE Photovoltaic Specialists Conference*, 1985, pp. 578–583.
[20] H. Mäckel and K. Varner, "On the determination of the emitter saturation current density from lifetime measurements of silicon devices," *Progress in Photovoltaics: Research and Applications*, vol. 21, no. February 2012, pp. 850–866, 2013.
[21] J. Swirhun, "PV Lighthouse: Spectrum Q-Flash," 2011. [Online]. Available: http://www.pvlighthouse.com.au/resources/optics/spectrum library/spectrum library.aspx
[22] A. Cuevas and R. A. Sinton, "Detailed modelling of the effective minority carrier lifetime and the open-circuit voltage of silicon solar cells," in *22nd European Photovoltaic Solar Energy Conference*, 2007, pp. 38–43.
[23] C. Reichel, F. Granek, J. Benick, O. Schultz-Wittmann, and S. W. Glunz, "Comparison of emitter saturation current densities determined by injection-dependent lifetime spectroscopy in high and low injection regimes," *Progress in Photovoltaics: Research and Applications*, vol. 20, no. 1, pp. 21–30, Jan. 2012.
[24] J. Greulich, U. Jäger, S. Rein, and R. Preu, "A Review and Comparison of One- and Two-Dimensional Simulations of Solar Cells Featuring Selective Emitters," *IEEE Journal of Photovoltaics*, vol. 2, no. 4, pp. 441–449, Oct. 2012.
[25] A. Sugianto, B. Tjahjono, J. Guo, and S. Wenham, "Impact of laser induced defects on the performance of solar cells using localised laser doped redions beneath the metal contacts," in *22nd European Photovoltaic Solar Energy Conference*, no. September, 2007, pp. 1759–1762.
[26] K. R. McIntosh and P. P. Altermatt, "A freeware 1D emitter model for silicon solar cells," in *35th IEEE Photovoltaic Specialists Conference (PVSC)*, 2010, pp. 2188–2193.
[27] L. Xu, K. Weber, A. Fell, Z. Hameiri, S. P. Phang, X. Yang, and E. Franklin, "The Impact of SiO 2 / SiN x Stack Thickness on Laser Doping of Silicon Solar Cell," *IEEE Journal of Photovoltaics*, vol. 4, no. 2, pp. 594–600, 2014.
[28] S. M. Hu, "Stress-related problems in silicon technology," *Journal of Applied Physics*, vol. 70, no. 6, pp. R53—-R80, 1991.
[29] S. C. Singhal, "Thermodynamic Analysis of the High Temperature Stability of Silicon Nitride and Silicon Carbide," *Ceramurgia International*, vol. 2, pp. 123–130, 1979.
[30] R. Pehlke and J. Elliott, "High-Temperature Thermodynamics of the Silicon, Nitrogen, Silicon-Nitride System," *Transactions of the Metallurgical Society of AIME*, vol. 215, pp. 781–785, 1959.
[31] J. Giesecke, *Springer Theses: Quantitative recombination and transport properties in silicon from dynamic luminescence*. Cham, Switzerland: Springer International Publishing, 2014.

Christian Geisler studied physics at the Georg-August-University in Göttingen, Germany, and received his diploma in 2010. Currently he is working toward the Ph.D. degree, studying laser processing for Ni–Cu plated silicon solar cells, within the division "Solar Cells – Development and Characterization" at the Fraunhofer Institute for Solar Energy Systems, Freiburg, Germany. His research interest include signal processing, laser structuring, and metal plating.

Sven Kluska received his diploma in physics and his Ph.D. in microsystems engineering at the Albert-Ludwigs University Freiburg in collaboration with Fraunhofer ISE, Germany. The focus of his work is the development and characterization of innovative process technologies for high efficiency silicon solar cells such as laser micro structuring, laser doping and Ni/Cu plating. Currently, he is working as post-doctoral fellow in the department for novel processes at Fraunhofer ISE.

Sybille Hopman was born in 1979. She studied process and environment engineering at the University of Applied Sciences in Offenburg, Germany. In 2011 she received her Ph.D. from the Albert-Ludwig-University of Freiburg, Germany, studying the application of laser chemical processing for high efficiency silicon solar cells. Since 2011 she is head of the team "Microstructuring and wet-chemical laser technologies" with the Fraunhofer Institute for Solar Energy Systems ISE, Freiburg, within the division "Solar Cells – Development and Characterization". Her current research interests include wet-chemical laser processing and novel manufacturing processes for crystalline silicon solar cells.

Johannes Giesecke was born in Berlin in 1981. He studied physics at the University of Konstanz, Germany, where he also received his PhD in physics in 2013 for his continuing work on dynamic luminescence techniques at Fraunhofer ISE.

Markus Glatthaar was born in 1975. He studied Physics at the Eberhard-Karls-University in Tübingen, Germany. In 2007 he received his Ph.D. in physics from the Albert-Ludwig-University of Freiburg, Germany, studying organic bulk heterojunction solar cells. From 2008 to 2010 he worked as a postdoc at the Fraunhofer Institute for Solar Energy Systems ISE developing characterization methods for silicon solar cells such as luminescence imaging. In 2011 he joined RENA GmbH as senior solar cell technologist. Since 2012 he is head of the department "Novel Processes" within the division "Solar Cells – Development and Characterization" at Fraunhofer ISE. His current research focus is on novel manufacturing processes for crystalline silicon solar cells.